Time Homogenization of Al3003 H-18 foils undergoing metallurgical bonding using Ultrasonic Consolidation

Deepankar Pal and Brent E. Stucker
Department of Industrial Engineering, University of Louisville, KY 40292

Abstract

A dislocation density based finite element model was formulated and initially validated using published experimental data for simple shear deformation of a single crystal pure aluminum and uniaxial tension of bulk polycrystalline Al 3003-H18 alloy. The model was extended to predict the deformation behavior of 150µm Al 3003-H18 foils undergoing ultrasonic consolidation (UC). The simulated results were in good agreement with the experimental results for the evolution of linear weld density and embrittlement due to grain substructure formation. A novel time homogenization approach has been further formulated which significantly reduces the computational overhead. The time-homogenization approach uses the Almost Periodic Time Homogenization (APTH) operator based on an asymptotic Forward-Euler scheme for integrating the coarse time increments. The computational efficiency is proportional to the ratio of coarse to fine time scales.

Introduction

In the recent past, an increasing drive for developing solid state additive manufacturing processes has been observed. The advantage of these processes over melting based process such as selective laser melting and electron beam melting is that the mechanical properties of the base material can be improved due to mechanical working. Moreover, these processes can also be seen as a set of next generation processes which can uplift the current status of the embedded electronics and sensors technology to its next level. It is possible since solid state processes like UC are additionally equipped with subtractive machining capabilities to create internal features in an additive environment where the operating temperature is close to room temperature which is not detrimental for the placement of electronics and sensors as their functionalities are highly sensitive to heat. Therefore, as a direct result of ongoing research efforts in ultrasonic consolidation (UC) worldwide, it has become apparent that a new approach to modeling of UC bonding is needed. A model which provides a better understanding of the effects of process parameter changes on grain refinement, plastic deformation and bonding during UC will better enable researchers to predict which materials will bond, how the mechanical properties of UC-produced parts can be improved, and how to better design the next generation of UC equipment.

It has been already established that the fine-time scale Dislocation Density based Finite Element Method (DDCP-FEM) simulations [1-6] are well suited for predicting the physics of material deformation during UC. These simulations, however, are not ideal for predicting long term deformation behavior occurring during the course of UC due to a very small time step used in this set of simulations and a relatively large problem size with intricate meshing. Hence, it is highly beneficial to jump an integral number of cycles over fewer time steps (e.g. time homogenization) while keeping the spatial fine-scale model results the same. In this way, the fine spatial scale information will be intact with a tremendous amount of computational efficiency in

processing and a small output matrix size to be post-processed for animations and visualizations. This can be possible with the use of the Almost Periodic Time Homogenization Operator (APTH) Ξ [7]. The APTH operator is applicable for history-dependent plasticity problems whereas simplified operators do exist for linear elastic problems [8]. The use of the APTH operator is straightforward for continuum plasticity scenarios [7] whereas for crystal plasticity the method presents challenges in terms of tracking all the 12 slip systems separately and their coarse time scale evolutions. Henceforth, a detailed mathematical formulation has been performed to incorporate the long term deformation behavior in UC.

Problem Formulation

1. Coarse-time scale Constitutive modeling

The principle of APTH states that the rate of change of macro-time scale arbitrary variable $\Xi(\varphi)$ is equal to the average rate of change of the arbitrary variable (φ) in the macro-time scale (t). This can be mathematically expressed as follows:

$$\frac{d(\Xi(\varphi))}{dt} = \langle \frac{d(\varphi)}{dt} \rangle \tag{1}$$

The macro-time scale evolutions of dislocation-density based constitutive variables are expressed in equations (2)-(7). The macro-time scale shear strain rate (rate over the coarse macro-time scale) is given by:

$$\frac{d\Xi(\gamma^\alpha)}{dt} = \begin{cases} \frac{d\Xi(\gamma_0^\alpha)}{dt} \exp\left[\frac{-Q_{slip}}{K_B T}\left(1 - \frac{|\Xi(\tau^\alpha) + \widetilde{\tau^\alpha}| - \Xi(\tau_{pass}^\alpha)}{\Xi(\tau_{cut}^\alpha)}\right)\right] \text{sign}\left(\Xi(\tau^\alpha) + \widetilde{\tau^\alpha}\right) \\ \qquad\qquad\qquad\qquad if \left|\Xi(\tau^\alpha) + \widetilde{\tau^\alpha}\right| \geq \Xi(\tau_{pass}^\alpha) \\ 0 \qquad\qquad\qquad\qquad if \left|\Xi(\tau^\alpha) + \widetilde{\tau^\alpha}\right| \leq \Xi(\tau_{pass}^\alpha) \end{cases} \tag{2}$$

where the pre-exponential variable $\frac{d\Xi(\gamma_0^\alpha)}{dt}$ is the upper limit of the shear rate for the case where the Boltzmann factor (K_B) is equal to 1 in Equation (2). Q_{slip} is the activation energy for the dislocation to advance by a burgers vector distance in the slip direction. $\Xi(\tau^\alpha)$ measures the resolved coarse time scale stress on the slip system (α). T is the temperature in the local vicinity of the deformation zone.

The definition of $\frac{d\Xi(\gamma_0^\alpha)}{dt}$ is mathematically expressed in Equation (3). The $\Xi(\rho_P^\alpha)$ in Equation (3) is defined as the coarse scale time estimate of the variable ρ_P^α indicating the density of dislocations in-plane of the moving dislocation causing repulsive drag to its further motion. The constants used in Equation (3) such as c_1 and c_3 are defined in Table 5 [4].

$$\frac{d\Xi(\gamma_0^\alpha)}{dt} = \frac{K_B T}{c_1 c_3 G b^2}\sqrt{(\Xi(\rho_P^\alpha) + \widetilde{\rho_P^\alpha})} \tag{3}$$

Where G is the shear modulus of the single crystal (shear moduli remain the same in 44,55 and 66 directions for FCC materials) and b is the magnitude of the burger vector.

The coarse time scale passing stress variable,$\Xi(\tau_{pass}^\alpha)$, caused by the parallel dislocations

is shown in Equation (4)

$$\Xi(\tau_{pass}^{\alpha}) = c_1 Gb \sqrt{(\Xi(\rho_P^{\alpha}) + \widetilde{\rho_P^{\alpha}})} \qquad (4)$$

Similarly, the cutting stress, τ_{cut}^{α}, at 0K caused by the forest dislocations

$$\Xi(\tau_{cut}^{\alpha}) = \frac{Q_{slip}}{c_2 c_3 b^2} \sqrt{(\Xi(\rho_F^{\alpha}) + \widetilde{\rho_F^{\alpha}})} \qquad (5)$$

where $(\Xi(\rho_F^{\alpha}))$ indicates the density of dislocations out-of-plane of the moving dislocation causing repulsive drag to its further motion due to dislocation looping effect [4].

The incompatibility in plastic deformation gradient and nonlocal geometrical nonlinearity is introduced using ρ_{GND}^{α} which computes the geometrically necessary dislocations required to maintain continuity throughout the material. The evolution law for ρ_{GND}^{α} [4] becomes

$$\frac{d\Xi(\rho_{GND}^{\alpha})}{dt} = \frac{1}{b} \left\| \nabla_X \times \left(\frac{d\Xi(\gamma^{\alpha})}{dt} + \widetilde{\dot{\gamma}^{\alpha}} \right) (\Xi(F_P^T) + \tilde{F}_P^T) \tilde{n}^{\alpha} \right\| \qquad (6)$$

Material hardening at an integration point is both a function of ρ_{GND}^{α} and ρ_{SSD}^{α} (statistically stored dislocation density). The evolution laws for ρ_{SSD}^{α} [4] are generally linear in shear rate.

$$\frac{d\Xi(\rho_{SSD}^{\alpha})}{dt} = c_4 \sqrt{(\Xi(\rho_F^{\alpha}) + \widetilde{\rho_F^{\alpha}})} \left(\frac{d\Xi(\gamma^{\alpha})}{dt} + \widetilde{\dot{\gamma}^{\alpha}} \right) - c_5 \left(\Xi(\rho_{SSD}^{\alpha}) + \widetilde{\rho_{SSD}^{\alpha}} \right) \left(\frac{d\Xi(\gamma^{\alpha})}{dt} + \widetilde{\dot{\gamma}^{\alpha}} \right) +$$
$$c_6 d_{dipole}^{\alpha} (\Xi(\rho_{mobile}^{\alpha}) + \tilde{\rho}_{mobile}^{\alpha}) (\frac{d\Xi(\gamma^{\alpha})}{dt} + \widetilde{\dot{\gamma}^{\alpha}}) - c_7 \exp\left(-\frac{Qbulk}{K_B T} \right) \frac{|\Xi(\tau^{\alpha}) + \widetilde{\tau^{\alpha}}|}{K_B T} (\Xi(\rho_{SSD}^{\alpha}) +$$
$$\widetilde{\rho_{SSD}^{\alpha}})^2 (\frac{d\Xi(\gamma^{\alpha})}{dt} + \widetilde{\dot{\gamma}^{\alpha}})^{c_8} \qquad (7)$$

It should be also noted that the time derivatives of $(\Xi(\varphi))$ are taken with respect to the macro-time scale (t).

The full fine-scale variable $(\tilde{\varphi})$ will be obtained from the micro-time scale simulations after subtracting the average variables ($<\varphi>$) from macroscopic variables $(\Xi(\varphi))$. Assuming, φ to be a variable of interest such as forest dislocation density(ρ_F^{α}), parallel dislocation density (ρ_P^{α}) or shear strain rate on a slip system$(\dot{\gamma}^{\alpha})$, the fine scale evolution with respect to micro-time scale (τ) can be computed as:

$$\frac{d\tilde{\varphi}}{d\tau} = \left(\frac{\tau}{t} \right) \left[\Xi\left(\frac{d\varphi}{dt} \right) - \langle \frac{d\varphi}{dt} \rangle_{\tau} \right] \qquad (8)$$

where $\Xi\left(\frac{d\varphi}{dt} \right)$ computes the macroscopic rate of change of the variable φ and $\langle \frac{d\varphi}{dt} \rangle_{\tau}$ computes the average macroscopic rate of change (average rate of change $\langle \frac{d\varphi}{dt} \rangle_{\tau}$ computed after taking the

difference of two consecutive fine time scales with oscillatory boundary conditions only) of the variable φ at fine-time scale (τ).

The fine scale variables are computed to inform the macro-time scale variables of the fine-scale counterparts and then the macro-time scale variables evolve per cycle (or integral number of cycles) as shown in equations (2)-(7). In each macro-time scale, the fine time scale variables are updated using equation (8). After a considerable number of cycles, the fine scale is again solved to update the oscillatory or fine-time scale counterparts and repeated over again till the total time reaches the end of the computational experiment.

2. Input process parameters

In this study, UC oscillation amplitude is set to 10 µm with a normal force to 1450 N and weld speed of 28 mm/s (see Table 8, entry column 1 in [4]) which is set of parameters which leads to poor bonding linear weld density [3]. The contact width calculated using the Hertzian contact equation [9] was 282 µm. Henceforth, the dimensions of the samples were fixed at 300 µm (2×UC foil thickness)×282 µm (contact width)×300 µm. The sonotrode operating frequency is 20kHz leading to a time period per oscillation of 50µs. Using the weld speed, the sonotrode residence time has been calculated ~10 milliseconds or 200 vibration cycles over the consolidation contact volume. The roughness at the top surface of the bottom foil [4] due to previous consolidation creates an average roughness of ~5 µm which has also been incorporated in the model as an input boundary condition. The input process parameters and initial model geometry have been shown in figure 1.

3. Modified Boundary Conditions

The simulation is divided into two parts namely the average and the oscillatory parts. The oscillatory part provides the fine time-scale information to be incorporated in the average macro coarse-time scale problem. The oscillatory part has been solved only with the simple shear boundary condition whereas the average part has been solved with the compressive load (pressure) boundary condition (figures 1 and 2).
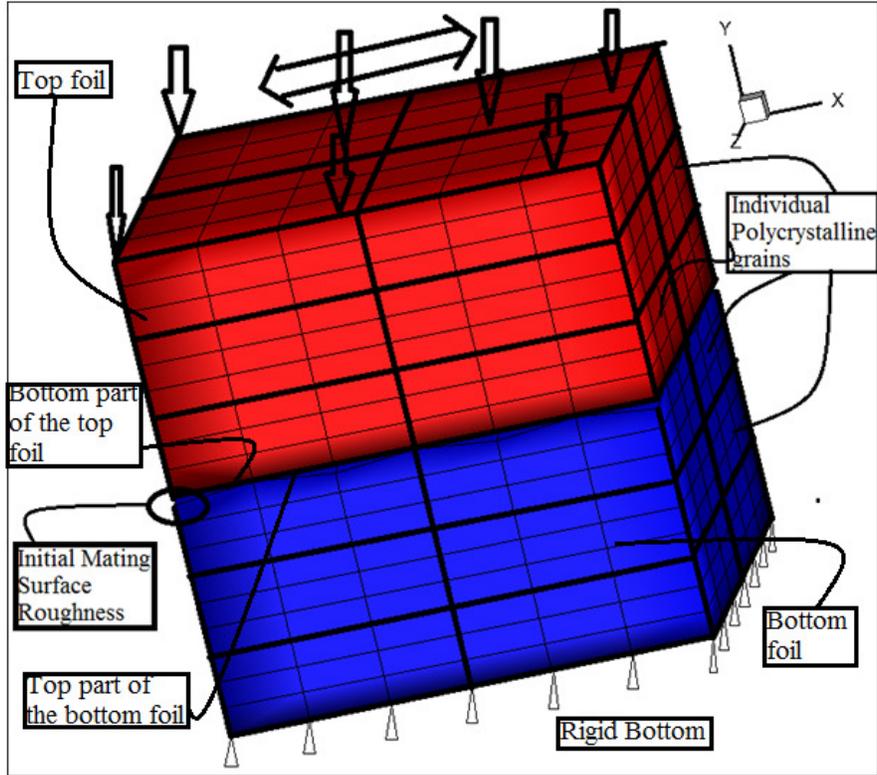
Figure 1. Schematic showing Ultrasonic Consolidation global boundary conditions on a small section of the actual mesh. The bottom of the model is held rigid. The average or coarse-time scale simulations only consist of the 'normal compressive' boundary conditions ($\downarrow$) and the oscillatory part consist of the 'simple shear' ($\leftrightarrow$) boundary conditions. The plastic variables of the oscillatory part are recorded after consecutive full cycles and then deducted from one another to obtain the average rate of change of the plastic variable $\langle\frac{d\varphi}{dt}\rangle_\tau$(Equation 8). This is deducted from the average problem $\Xi\left(\frac{d\varphi}{dt}\right)$ (Equation (8)) to obtain the $\frac{d\tilde{\varphi}}{d\tau}$ (Equation 8) which computes the full fine-time scale variation of the variable (φ) for any time (τ) such that τ lies in between any two deformation cycles with both normal compressive and simple shear boundary conditions.
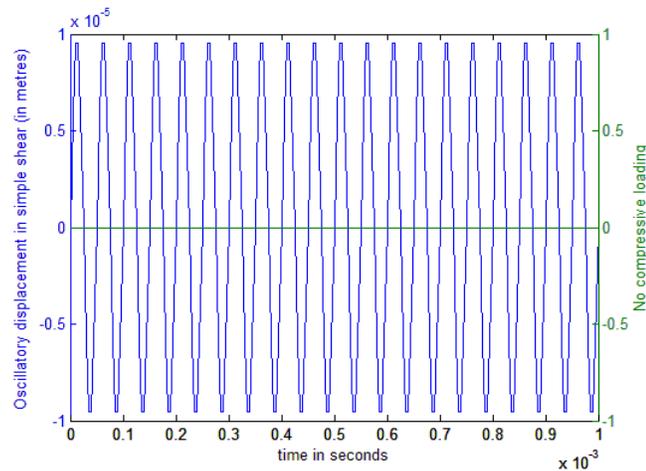
(a)
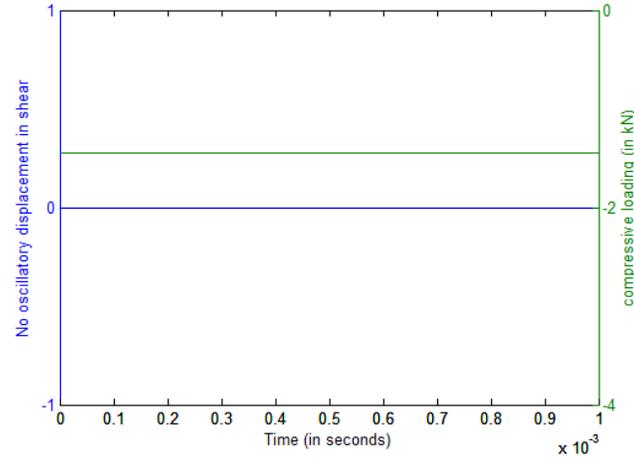
(b)
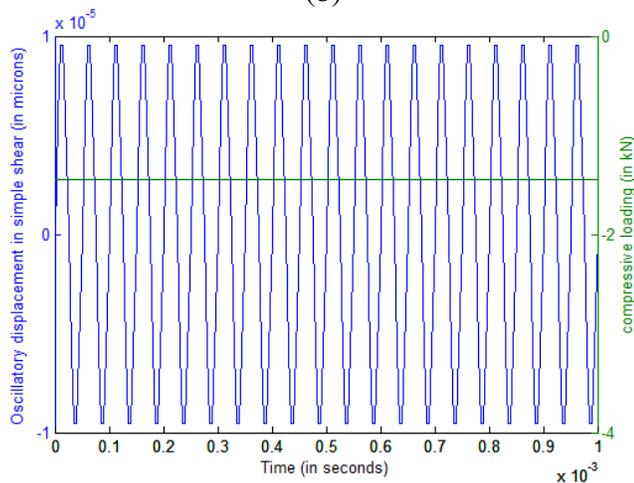
(c)

Figure 2 (a) shows the oscillatory shear boundary condition with no compressive loading to be solved in fine time scale, (b) shows the coarse-scale constant compressive loading to be solved in coarse-time scale, (a+b) represent the modified boundary conditions in section 3 whereas (c) provides with combined boundary conditions to be solved in fine–time scale used to be solved earlier and further discontinued for CPU memory usage.

Results and Discussion

1. Lattice Curvature Evolution

The fine-time scale evolutions mentioned in [6] have been incorporated for the coarse-time scale problem with the compressive load boundary condition. Since, the GND computes the incompatibility in the continuity of the crystal, a higher GND leads to larger incompatibility in continuity throughout the crystal. An increase in GND is directly proportional to intragranular misorientations ($>15^o$) leading to grain fragmentation. It has been observed during the course of simulation that the GND starts building up significantly at the top surface of the bottom foil leading to grain fragmentation. As the number of cycles increase, the interfacial aspects of UC also continuously change. The initial frictional sliding gradually changes to a foil sticking scenario (~50 cycles) and GND starts to develop in the top surface of the top foil along with the top surface of the bottom foil. By the end of deformation cycles in the representative volume

element, the top surfaces of both the top and bottom foils will be covered with fragmented grains due to the huge magnitude of GND evolution. In order to fully understand the long term deformation behavior in UC, more cycles have been simulated, though the deformation aspects have saturated after the top and bottom foils come in contact (it should be noted that there is no crack propagation or low cycle fatigue failure mechanism currently in the model). GND evolution as a function of increasing number of cycles is shown in Figure 4 (a-h). The regions of higher GND evolutions are in well agreement with experimentally observed miscrostructures shown in figure 5. The initially fragmented grain patches near the top surface of the bottom foil during the frictional sliding stage are clearly visible in Figure 5(a). Similarly, the fragmented grain patches which are in direct contact with the sonotrode are illustrated in Figure 5(b). The grain fragmentation in Figure 5(a) is much finer than Figure 5(b) due to its earlier initiation during the UC processing. All top surfaces of consolidated foils are equally fragmented since the foils are laid one upon each other to fabricate a 3 dimensional part.
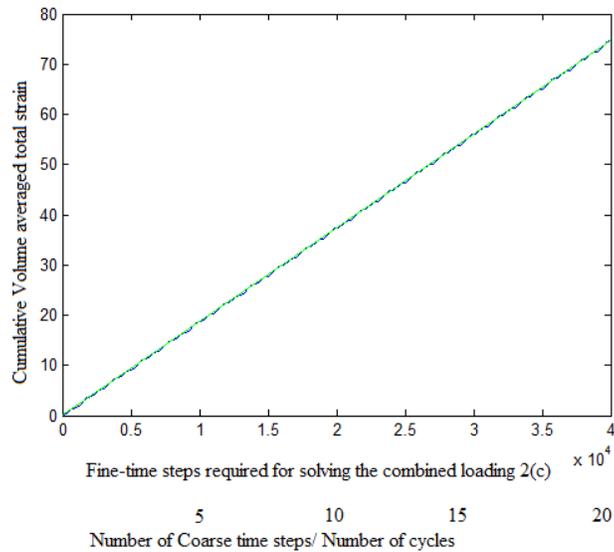

Figure 3. Comparison between full fine time scale combined boundary condition (figure 2(c)) simulation (blue) and coarse time scale (figure 2(a+b) simulation (red) at the end of 20 cycles. Full fine time scale takes 2000 times slower as compared to the coarse time scale simulations.
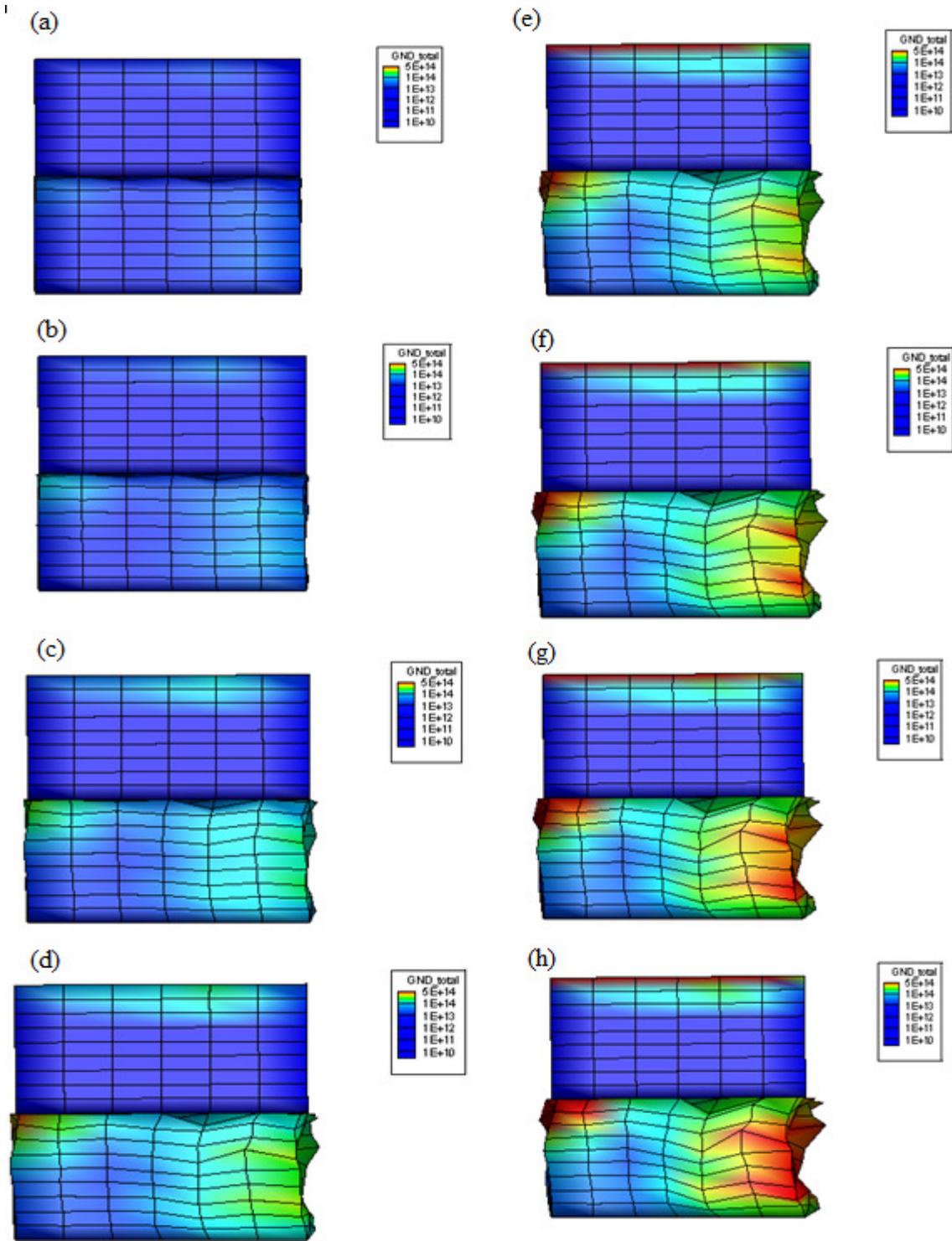
Figure 4. GND evolutions at (a) 10, (b) 20, (c) 50 ((i) onset of significant GND evolution: top surface-top foil and (ii) frictional sliding to sticking), (d) 80, (e) 100, (f) 120, (g) 140 and (h) 160 cycles. CPU time advantage attained is 2000:1.
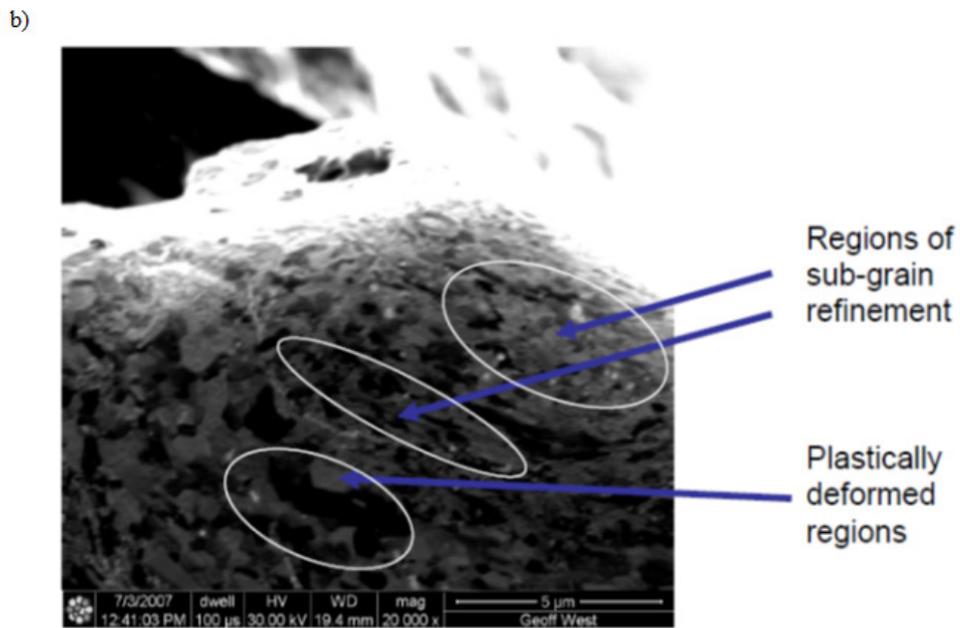
a)

Nano-grain colonies

b)

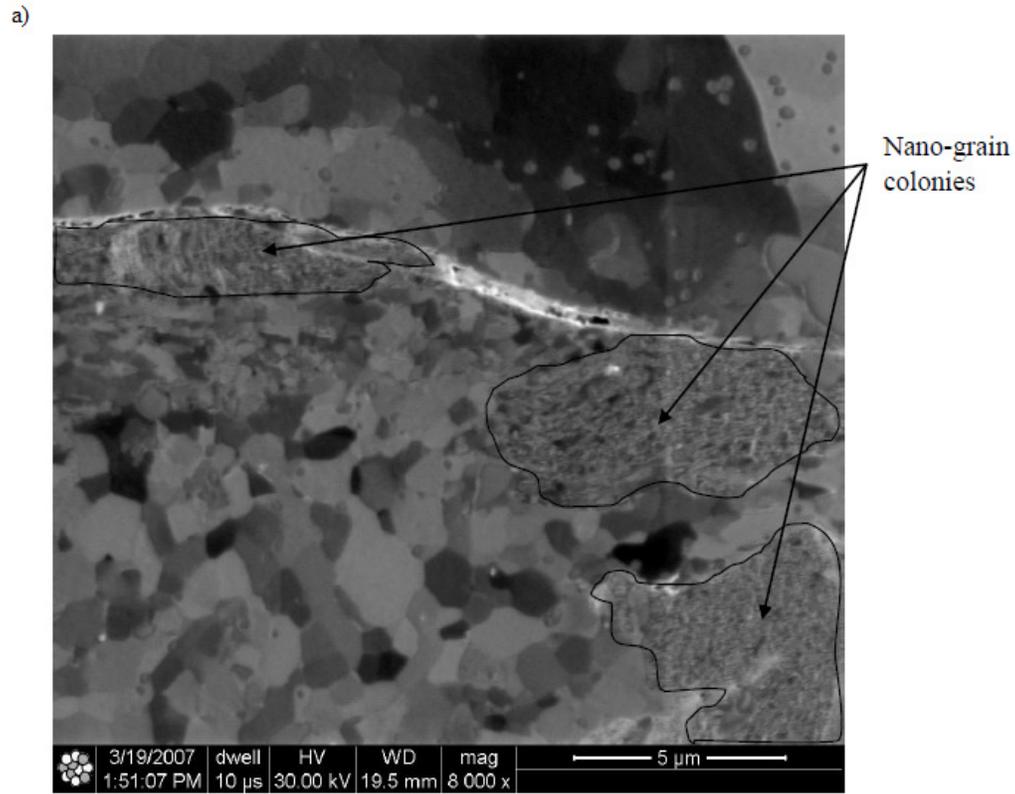Regions of sub-grain refinement

Plastically deformed regions

Figure 5. Ion beam induced secondary electron micrograph of (a) UC interface region showing nano-grain colonies (*i.e.* regions of dense nano-grain sized sub-grains) outlined [10] and (b) top of welded foil layer that experienced direct sonotrode contact

2. Gap Evolution (Rate of Ultrasonic 'Consolidation')

It is important to quantify the amount of gap between two foils as a function of increasing deformation cycles. An initial gap region is present between the top and bottom foils due to sonotrode-induced surface roughness on the top surface of the previously deposited (e.g. bottom) foil. This gap tends to close with increasing number of cycles, though the rate at which the gap is closed tends to slow down with increasing number of cycles due to increasing plasticity per cycle (figure 6).
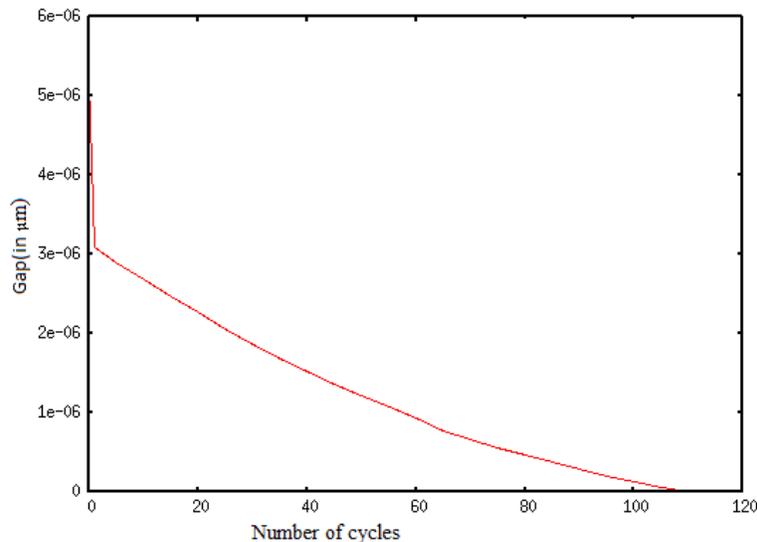

Figure 6. Gap evolution as a function of number of cycles.

Conclusions

The APTH operator used in the present study successfully described the long term plastic deformation behavior (low cycle fatigue). The following are the major inferences made by incorporating the APTH operator in this exercise:

- The initial macroscopic deformation mode at the UC interface is frictional sliding
- With increasing number of deformation cycles the interlayer gap comes down and the deformation mode at the UC interface changes to sticking.
- The interlayer gap takes a significant number of cycles to close. The rate of gap closure slows down with increasing number of cycles, since the amount of cumulative plastic deformation increases in the representative volume.
- GND or lattice curvature evolves significantly only near the top surface of the bottom foil due to the initial sliding deformation mode at the UC interface which further extends to the top surface of the top foil as the deformation mode changes from sliding to sticking. This leads to the conclusion that grain fragmentation will be more significant near the top surface of the bottom foil at the UC interface when compared to the top surface of the top foil. Due to the fact that the sheets will be laid one upon another during ultrasonic consolidation, the top surfaces each subsequent foil layer will have an equal amount of

grain fragmentation in the finally consolidated UC part, except the last layer to be deposited.

The methodology shown in this paper can be easily extended to a range of materials undergoing UC or a different set of boundary conditions since the material variables required for simulating a new material can be obtained from fundamental calculations as shown in Table 5 [4] with an update on the crystal structure leading to a different set of slip system orientations and initial dislocation densities [11].

Acknowledgements

References

1. Pal, D., Behera, S. and Ghosh, S. Crystal Plasticity Modeling of Creep and Microtwinning in Nickel based Superalloys, *United States National Congress on Computational Mecha*nics, Columbus, OH, July 2009.
2. Pal, D. and Stucker, B.E. Dislocation Density Based Finite Element Modeling of Ultrasonic Consolidation, *Solid Freeform Fabrication Symposium Proceedings*, 2010, Austin, TX, August 2010.
3. Pal, D. and Stucker, B.E. Dislocation Density Based Finite Element Modeling of Ultrasonic Consolidation, *Solid Freeform Fabrication Symposium Proceedings*, 2011, Austin, TX, August 2011.
4. Pal, D. Dislocation Density-Based Finite Element Method Modeling of Ultrasonic Consolidation, Ph.D Thesis, Utah State University, August 2011.
5. Pal, D., and Stucker, B.E. Some Studies on Dislocation Density Based Finite Element Modeling of Ultrasonic Consolidation, *Proceedings of the 5th International conference on Virtual and Rapid Prototyping*, Leiria, Portugal, 2011.
6. Pal, D., and Stucker, B.E. Modeling of Ultrasonic Consolidation Using a Dislocation Density Based Finite Element Framework, *Virtual and Physical Prototyping Journal*, Volume 7(1), pp. 65-79.
7. Oskay, C., and Fish, J. Fatigue Life Prediction Using 2-scale Temporal Asymptotic Homogenization, *International Journal of Numerical Methods in Engineering*, Volume 61(3), pp. 329-359, 2004.
8. Yu, Q., and Fish, J. Multiscale asymptotic homogenization for multiphysics problems with multiple spatial and temporal scales: A coupled thermo-viscoelastic example problem, *International Journal of Solids and Structures*, Volume 39(26), pp. 6429-6452.
9. Hertz, H.R., Ueber die Beruehrung elastischer Koerper (On Contact Between Elastic Bodies)*, in Gesammelte Werke (Collected Works)*, Vol. 1, Leipzig, Germany, 1895.
10. Johnson, K.E. Interlaminar Subgrain refinement in Ultrasonic Consolidation, Ph.D. Thesis, Loughborough University, May 2008.
11. Pal, D., Patil, N., and Stucker, B.E. Prediction of mechanical properties of Ti64AlV parts

produced using Electron Beam Melting, *Solid Freeform Fabrication Symposium Proceedings*, 2012, Austin, TX, August 2012 (in communication).